Self-interstitial solute complexes in e^--irradiated dilute Al-Ag and Al-Si alloys

E. C. Johnson*
Department of Physics and Materials Research Laboratory, University of Illinois at Urbana-Champaign, Urbana, Illinois 61801

A. V. Granato
Department of Physics and Materials Research Laboratory, University of Illinois at Urbana-Champaign, Urbana, Illinois 61801† *and Center for Materials Science, Mail Stop K-765, Los Alamos National Laboratory, Los Alamos, New Mexico 87545*

(Received 27 July 1987; revised manuscript received 4 April 1988)

Ultrasonic attenuation and velocity measurements were performed to probe the structure and annealing behavior of self-interstitial solute complexes in electron-irradiated ($T < 70$ K) dilute Al-Ag and Al-Si alloys. In both alloy systems, a similar attenuation peak structure is observed. Three peaks are observed to anneal in unison during stage II, suggesting that they arise from the presence of a single defect structure. The annealing of this defect structure follows a first-order rate equation which has a prefactor proportional to the solute concentration. The diaelastic effect associated with this defect is found to be comparable in magnitude and anisotropy to that attributed to ⟨100⟩ self-interstitial dumbbells in pure aluminum. A ⟨110⟩ monoclinic mixed dumbbell model which can account for much of the observed behavior of this defect structure is proposed.

I. INTRODUCTION

A number of radiation-damaged, dilute Al-alloy systems have been examined ultrasionically in an effort to understand the basic nature of self-interstitial–solute (SIS) interactions. Early studies revealed an ultrasonic attenuation peak structure much more diverse than that expected on the basis of computer simulations.[1] Each alloy was characterized by a distinct peak structure bearing little resemblance to each of the others studied. The ⟨100⟩ mixed dumbbell structure, which was expected to occur most readily, was only confirmed in the case of Al-Zn.[2] Recently, however, it was reported that the peak structure which arises as a result of e^- irradiation in Al-Si is very similar to that of Al-Ag.[3] In addition, recent internal friction measurements in polycrystalline Al alloys have revealed that a similar peak structure is also found in fast-neutron-irradiated Al-Ag, Al-Si, Al-Pb, Al-Sn, and Al-In.[4] In this paper, the results of a more detailed study of Al-Ag and Al-Si will be presented. These results will then be compared with what has been found by empolying different techniques. Finally, a defect model will be presented which can account for much of the observed behavior.

The present ultrasonic study was performed on electron-damaged, single-crystal, bulk specimens. Electrons were used because they produce simple damage, consisting mainly of isolated Frenkel pairs. This study is characterized by several advantages. Most significantly, detailed symmetry information can be deduced about each defect complex from the polarization dependence of its response to strain.[5] In addition, the response of each type of defect species, when several are present simultaneously, can be studied independently. Often, defect concentrations of ≈ 1 ppm are sufficient for ultrasonic study, so that problems associated with high defect concentrations can be avoided.

II. EXPERIMENT

A. Sample preparation

Single-crystal, cylindrical (1.9 cm diameter) boules of Al-Ag and Al-Si were purchased from Monocrystals Company of Cleveland, Ohio. Using the Laue double-exposure scheme developed by Ochs,[6] each boule was oriented within 0.5° of the [110] direction. An acid saw was used to cut a sample approximating a cube with edges of ≈ 1 cm from each boule. Two sets of (110) faces were electropolished flat and parallel to almost optical tolerances. The ultrasound was propagated between one set of faces, while the other set allowed for good thermal contact between the sample and sample holder. A quartz transducer was bonded to one of the ultrasonic faces with Nonaq stopcock grease, and aligned so as to produce the appropriate polarization of ultrasound. Four samples, each from a separate boule, were prepared. Each sample will be discussed separately below.

B. Apparatus

The pulse-superposition system, which was used for three of the four samples studied, permits one to measure both attenuation and velocity of ultrasonic pulses within a sample at two distinct frequencies simultaneously. A detailed description of this system can be found in the thesis work of W. Johnson.[7] The closed-cycle refrigerator-cryostat and sample holder used to study these three samples is discussed elsewhere[8] as is the method used for simultaneous impedance matching at two ultrasonic frequencies.[9] The remaining sample, Al–1280-ppm Ag, was the first studied and two MATEC, Inc. pulse generator-receiver units were used to measure attenuation only. In addition, a different cryostat[10] was used.

C. Technique

Following preparation, the sample was placed within the cryostat with the face opposite the transducer facing the electron beam. The ultrasonic attenuation and velocity were then measured as a function of sample temperature for $2 < T < 240$ K. The sample was then subjected to thermal cycling to test the extent to which the measurements would be affected by shifts in the bond. If the bond appeared to be of good quality, the sample was then irradiated with 2.5-MeV electrons while the sample temperature was held below 70 K. Following irradiation to a prescribed dose, the sample temperature was again lowered to ≈ 4 K. The temperature was then increased at a fixed rate (typically 1 K/min), to an isochronal anneal temperature T_A, with the velocity and attenuation being constantly monitored. The sample was then held at this temperature for 10 min before ramping back down. This process was then repeated for several successively increasing isochronal anneal temperatures. Finally, the sample was warmed to room temperature and then, if desired, the transducer was reoriented to produce a different polarization of ultrasound and the entire procedure repeated. The isochronal annealing temperatures were initially chosen to correspond to observed resistivity substages and then modified so as to best examine the annealing of the various radiation induced changes which were observed ultrasonically.

D. Dose determination

A 0.025-cm-thick foil was positioned directly in front of the sample throughout the irradiation. This foil was cut from the same boule as the sample. The resistivity change of the foil (assuming 0.0004 $\mu\Omega$ cm/ppm Frenkel pair[11]) was then used to calculate the volume-averaged Frenkel-pair (FP) concentration within the sample. The data for all the plots to be presented in this paper have been normalized to reflect a dose corresponding to 1 ppm FP.

III. Al–673-ppm Si RESULTS

A. Composition

For this sample, atomic-absorption-spectroscopy results indicated a Si concentration of 673±67 ppm. In addition, mass-spectroscopy results showed the concentrations of other trace impurities to be approximately 2 orders of magnitude less than this.

B. C' mode

Attenuation and velocity measurements were made at two frequencies, 10.86 and 30.87 MHz, simultaneously. The sample was irradiated with a dose corresponding to approximately 1.86 ppm FP. Following irradiation, one attenuation peak was detected with a peak temperature, $T_P = 20.33$ K for 10.86 MHz and $T_P = 22.33$ K for 30.87 MHz. The height of this peak was then monitored following several isochronal anneals. The 10.86-MHz peak and its associated velocity dispersion throughout the tempering treatment are plotted in Fig. 1. The logarithmic decrement δ is related to the measured attenuation α (in dB/μs) by the relation[12] $\alpha = 1.38/\omega\delta$, where ω is the angular frequency. The relative elastic modulus change is twice the relative velocity change ($\Delta C/C = 2\,\Delta v/v$). The $\Delta C/C$ curve reveals, in the (4–15) K range, a diaelastic change in the modulus, $\Delta C/C \approx 1.3\times 10^{-5}$ per 1 ppm FP, which appears to anneal in conjunction with the peak. Assuming an Arrhenius relaxation time ($\tau = \tau_0 e^{Q/kT}$), and that this is a Debye peak, one can determine Q and τ_0 from the shift in peak position with frequency.[5] Here one finds that $Q = 0.020 \pm 0.001$ eV and $\tau_0 = (0.92 \pm 0.1)\times 10^{-13}$ s. The ratio of the half-width determined experimentally to that expected for an ideal Debye peak with these parameters is $\Delta_{\text{expt}}/\Delta_D = 1.0 \pm 0.1$.

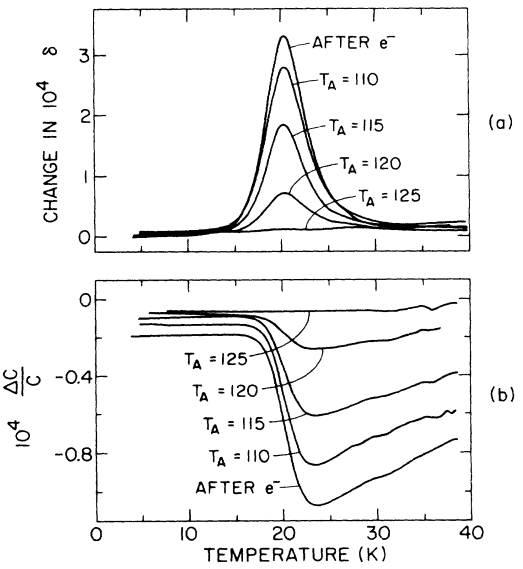

FIG. 1. (a) Al–673-ppm Si, 10.86-MHz, C' attenuation peak and (b) relative elastic constant change dispersion vs temperature following irradiation and after successive isochronal anneals at $T = T_A$. The results present after a 200-K isochronal anneal were subtracted from the raw data to produce these curves.

C. C_{44} mode

The C_{44} mode was studied twice. The first experiment suggested the need for a repeated study, with an increased electron dose. The results of the first study have already been reported.[3] The data presented here were obtained during the second run, where, as expected, the increased dose permitted better measurements. In this run, measurements were made at 11.0 and 30.47 MHz simultaneously. The sample was irradiated to approximately 4.7 ppm FP. Following irradiation, an attenuation peak with peak temperature, $T_P = 101.4$ K for 11.0 MHz and $T_P = 110.4$ K for 30.47 MHz, was detected. This peak will be referred to as C_{44}-1. The $\Delta C/C$-versus-T background curve has a steep slope throughout the temperature range spanned by this peak, making it quite a challenge to measure small relative elastic-constant changes. A successful measurement, however, was accomplished

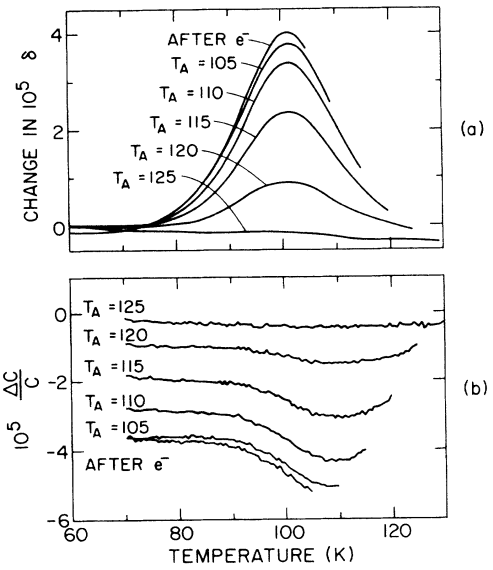

FIG. 2. (a) Al–673-ppm Si, 11.0-MHz, C_{44}-1 attenuation peak and (b) associated relative elastic constant dispersion following irradiation and after successive isochronal anneals at $T=T_A$. These curves reflect changes relative to what was present following a final 150-K anneal.

for the 11.0-MHz signal.

In Fig. 2 the 11.0-MHz attenuation peak and its associated velocity dispersion following irradiation and several isochronal anneals are plotted against temperature. In addition, several of the decrement curves [Fig. 2(a)] have been shifted in temperature so that they match up below the peak. This shift serves to cancel effects due to changes in the sample conductivity and shifts due to bond changes. The $\Delta C/C$ curves in Fig. 2(b) have not been shifted so as to reveal the diaelastic change, $\Delta C/C \approx 3.5\times10^{-5}$ per 1 ppm FP. For this peak, $\tau_0=(5.5\pm0.1)\times10^{-14}$ s, $Q=0.109$ eV, and $\Delta_{\text{expt}}/\Delta_D = 1.0\pm0.01$.

In addition to the peak described above, one or more very small peaks, which will be referred to as C_{44}-2, were detected near 30 K. The 11.0-MHz data were rather poor, serving mainly to confirm the effect seen in the 30.47-MHz data and to suggest the possible existence of multiple peaks. The 30.47-Mhz data are depicted in Fig. 3. The C_{44}-1 and C_{44}-2 peaks appears to anneal in unison.

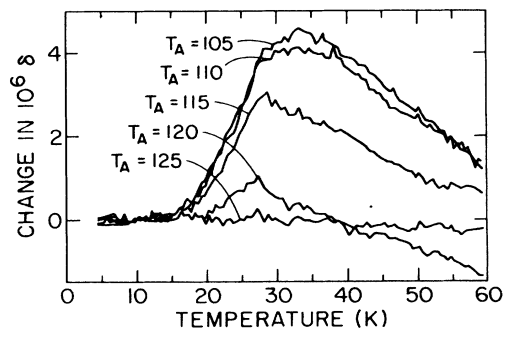

FIG. 3. Al–673-ppm Si, 30.47-MHz, C_{44}-2 peak(s) after successive isochronal anneals at $T=T_A$. These curves have been arbitrarily shifted to zero at 11 K. The decrement changes are relative to a final 150-K anneal. Note that the annealing of this peak(s) is very similar to that of C_{44}-1 depicted in Fig. 2. The decrement changes are relative to a final 150-K anneal.

D. Isothermal annealing of the C_{44}-1 peak

For the 30.47-MHz signal, significant annealing of the C_{44}-1 peak occurred during its measurement. It was possible, therefore, to monitor the peak height, as a function of time, while the sample temperature was maintained for 10 min at each T_A. One method for analyzing this isothermal annealing data is suggested by a brief consideration of first-order kinetics as discussed by Granato and Nilan.[13]

For particles climbing out of a potential well over a barrier of height E_M, and reaching a sink after N equivalent jumps, one has the expression

$$\frac{dc}{dt} = -(cv/N)\exp(-E_M/kT)\ , \tag{1}$$

where c is the concentration of particles in the well, the derivative is with respect to time t, v is the attack frequency, k is Boltzmann's constant, and T is temperature (K). One observes first-order kinetics when N is a constant. The 30.47-MHz isothermal annealing data fitted to Eq. (1) yielded the parameter values $E_M=0.234$ eV and $v/N=(5.99\pm0.12)\times10^6$ s^{-1}. A more detailed analysis of these data is presented in the thesis work of E. Johnson.[14]

E. Isochronal annealing

In Fig. 4 the percentage of the initial peak height remaining after each anneal is plotted against the isochronal anneal temperature for the C' and C_{44}-1 and peaks. In addition, a calculated curve using the parameters determined from the C_{44} data assuming a first-order process is included. This curve was computer generated

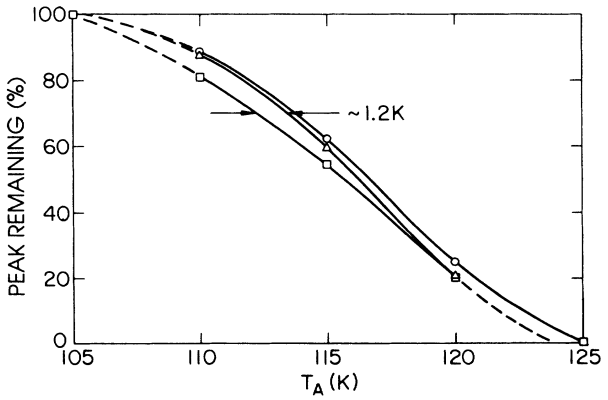

FIG. 4. For Al–673-ppm Si, the precent age of peak height remaining after successive 10-min isochronal anneals at $T=T_A$ for the C' peak (□), C_{44}-1 (○), and that predicted using the first-order parameters, $E_M=0.234$ eV and $v/N=(5.99\pm0.12)\times10^6$ s^{-1} (△).

and includes effects due to annealing during the ramp up and down from the anneal temperature. This curve approximates the actual data reasonably well. In addition, it can be noted, that the C_{44}-1 peak annealing parallels that of the C', peak lagging behind it by less than 1.2 K. If one defect species is responsible for both peaks, one would expect both peaks to anneal together. The difference is small enough, however, that it might be due to experimental error, reflecting the fact that it is very difficult to exactly duplicate conditions for two separate irradiation-annealing runs.

In an attempt to determine whether or not C_{44}-1 and the C' peak anneal concurrently, an experiment was performed using $\langle 110 \rangle$ propagating longitudinal ultrasound. The elastic constant associated with this pure mode is $C_L = C_{44} + C'/3 + B$, where B is the bulk modulus. Consequently, both peaks were observed simultaneously in the same mode. The results of this experiment have already been reported.[15] The measurements indicated that the apparent lagging of the C_{44} peak annealing in Fig. 4 could be explained by the existence of another peak, which will be referred to as C_{44}-4, at a significantly higher temperature which grew in upon the annealing of this peak, and annealed away before being surmounted in these measurements.

IV. Al–36-ppm Si RESULTS

A. Composition

For this sample, atomic-absorption-spectroscopy results indicated a Si concentration of 36±18 ppm. In addition, a semiquantitative mass spectrographic analysis, whose results are estimated to be accurate within a multiplicative factor of 3, detected a Si concentration of 20.0 ppm and concentrations of 3.0, 8.0, 3.0, 5.0, 8.0, 5.0, 20.0, and 9.0 ppm for the trace impurities Zn, Cu, Ca, K, S, Mg, Na, and F. The relative purity of this sample is of particular interest because of the low concentration of the desired solute. Using 0.72 $\mu\Omega$ cm as the resistivity contribution per at. % Si in the aluminum lattice,[16] one can estimate the Si concentration from the height of the low-temperature attenuation background rise. The necessary equations are provided by Pippard[17] and an example calculation is included in the thesis work of Wallace.[18] In a preliminary 11.3-MHz measurement, the C' background rise was determined to be ≈ 1.34 dB/μs. If Si was the only impurity present, such a rise would indicate a 26 ppm concentration, so that the concentrations of trace impurities present probably fall on the low side of the mass-spectrographic results. The sample was prepared as described above, and measurements were made for the C' and C_{44} ultrasonic modes.

B. C' mode

As a result of the relative sample purity, the background attenuation was high and changed rapidly with temperature, making detection of the expected radiation-induced C' relaxation peak (near 20 K) too difficult. The velocity background, however, changes slowly with temperature near 20 K so that measurements

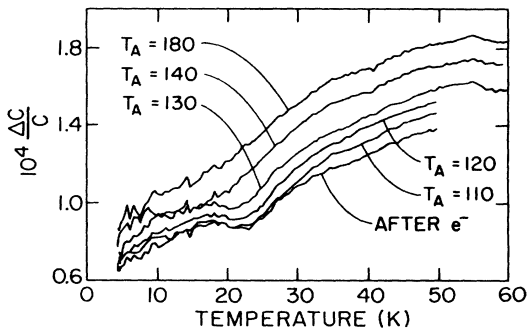

FIG. 5. Al–36-ppm Si, 10.3-MHz, C'-mode relative elastic constant dispersion after irradiation and successive isochronal anneals at $T = T_A$. These plots display changes relative to the preirradiation background.

of the radiation-induced relative elastic constant changes were possible, but quite noisy because the increased attenuation hindered the tracking capabilities of the pulse-superposition electronics.

The sample was irradiated to 2.4 ppm FP. Velocity measurements were made at 10.3 and 30.3 MHz simultaneously. In Fig. 5 the 10.3-MHz radiation-induced relative elastic-constant changes detected, following irradiation and several isothermal anneals, are plotted against temperature. As expected, a dispersion occurs near 20 K; however, it appears to be riding on the tail of a lower-temperature effect that was not detected in the Al–673-ppm Si sample. For the Al–673-ppm Si analysis, however, a suitable preirradiation background was not available, so that the radiation-induced changes were referenced to what was present following a 200-K anneal. Hence, this low-temperature effect may have been subtracted off, not having annealed before 200 K. Alternately, this effect may be due to one of the trace impurities. One might note that a significant portion of the dispersion is still present following isochronal anneals at temperatures for which that of the Al–673-ppm Si sample had already disappeared. This change in annealing with dopant concentration was also observed in the C_{44}-mode results and will be discussed after the C_{44} results are presented.

C. C_{44} mode

Following irradiation to a dose corresponding to 2.26 ppm FP, C_{44} attenuation measurements were made at 12.9 and 34.72 MHz simultaneously. Changes in the log decrement following irradiation, and after several 10-min isochronal anneals, are plotted against temperature for the 12.9-MHz signal in Fig. 6. The decrement, activation energy, and relaxation time determined from these data are consistent with that determined for the C_{44}-1 peak in the Al–673-ppm Si sample. It also appears that this peak is riding on the tail of another higher-temperature peak (C_{44}-4) that annealed away before being surmounted in these measurements, as was suggested by the C_L-mode results discussed above. In this case, the effects of this higher-temperature peak might be more pronounced be-

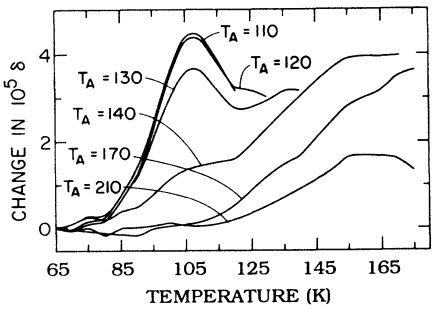

FIG. 6. Al–36-ppm Si, 12.9-MHz, C_{44}-1 peak after irradiation and successive isochronal anneals at $T=T_A$. These plots display changes relative to the preirradiation background.

cause the annealing of the C_{44}-1 peak occurs at a higher temperature.

D. Annealing

The percentage of the initial C_{44}-1 peak height remaining in Fig. 6, and the percentage of the C' dispersion (Fig. 5) remaining are plotted against T_A in Fig. 7. The fact that these two plots fall on top of each other, and the fact that in each case there has been an equal shift of $\approx$20 K in annealing temperature with decreased solute concentration, provide strong evidence that the same defect species is responsible for both the C' and C_{44}-1 peak, as was suggested by the C_L-mode results.

The isochronal annealing curves for Al–673-ppm Si (Fig. 4) were well approximated by Eq. (1), with E_M and v/N determined from the isothermal anneals. These values were used to calculate the annealing curve expected for the annealing program to which the Al–36-ppm Si sample was subjected. This calculated curve is plotted in Fig. 7, and can be seen to significantly precede the actual results in temperature. In order to explain the shift in annealing with solute concentration, one might assume that, given sufficient thermal energy, the defect complex responsible for both peaks migrates within the lattice until

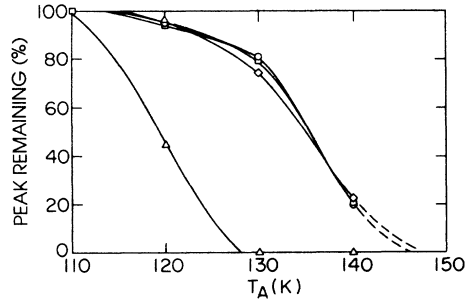

FIG. 7. Al–36-ppm Si. Percentage of the initial peak height remaining after each isochronal anneal at $T=T_A$ for C_{44}-1 (□), the C' peak (○), that expected on the basis of the first-order annealing parameters determined for Al–673-ppm Si (△), and that expected if one multiplies the prefactor v/N by the solute concentration ratio 36/673 (◇).

it encounters a substitutional Si atom and is trapped. The average number of equivalent jumps, N, executed by the defect before reaching a sink, would then be proportional to the concentration of Si in the lattice. Multiplying the prefactor v/N obtained for Al–673-ppm Si by the concentration ratio, 36/673, and recalculating the expected annealing curve for the Al–36-ppm Si sample gives a result very close to that obtained experimentally as depicted in Fig. 7.

V. Al–1280-ppm Ag RESULTS

A. Composition

A portion of this sample was analyzed by flame emission three times. The results indicated a Ag concentration of 1280±100 ppm with a standard deviation of less than ±55 ppm among the six measurements made for each analysis. In addition, a semiquantitative mass-spectrographic analysis indicated that the Ag concentration was between 130 and 1200 ppm and that the concentrations of other trace impurities were approximately 2 orders of magnitude less than that of the Ag. Another portion of the boule from which this sample was cut was subjected to neutron-activation analysis and thereby determined to contain 555.3±22.5 ppm Ag, indicating the existence of a significant concentration gradient within the sample. Taking the resistivity contribution for Ag in aluminum to be 1 $\mu\Omega$ cm per at. %, the volume-averaged Ag concentration was estimated from the background attenuation to be 1126±273 ppm. This value is the average of that obtained from the C' mode at 10.09 MHz and C_{44} mode at 10.87 MHz.

B. C' mode

For the C' mode, attenuation measurements were made at 10.09 and $\approx$30 MHz simultaneously. The sample was irradiated with a dose corresponding to 2.1 ppm FP. Following irradiation, a peak was detected at $T_P\approx$21.2 and 23.3 K for 10.09 and $\approx$30 MHz, respectively. For this peak one obtains $Q=0.022$ eV and $\tau_0=0.92\times10^{-13}$ s.

C. C_{44} mode

Measurements of the C_{44}-mode attenuation were made at 10.87 MHz and a frequency near 30 MHz simultaneously. The sample was irradiated with a dose corresponding to 1.8 ppm FP. Following irradiation, a peak was detected at $T_P\approx$103.2 and 113.2 K for 10.87 and $\approx$30 MHz, respectively. The $\approx$30-MHz radiation-induced decrement change is plotted in Fig. 8 following several successive isochronal anneals. The T_P values given above include a correction for a 1.6-K thermal lag between the sample and thermometer. For this peak one obtains $Q=0.103$ eV and $\tau_0=1.37\times10^{-13}$ s. It appears that this peak, like C_{44}-1 in Al-Si, is also riding on the tail of a higher-temperature peak that annealed away before it was surmounted. Since the situation is very similar to that of Al-Si, this peak will also be referred to as C_{44}-1. Correcting for the higher-temperature peak, the

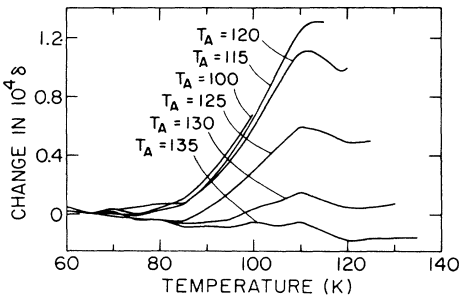

FIG. 8. Al–1280-ppm Ag, 30.0-MHz, C_{44}-1 peak after irradiation and successive isochronal anneals at $T=T_A$. These plots display changes relative to the preirradiation background.

half-width approximates that expected for a Debye peak with an Arrhenius relaxation time.

In addition to the two peaks mentioned, a very small peak ($\delta\approx 6.3\times 10^{-6}$ normalized to 1 ppm FP) was detected near 20 K immediately after irradiation. This peak had changed little following a 180-K anneal, but was nearly gone following a 220-K anneal. The dose was insufficient for a careful analysis of this peak. This peak was also detected in the Al–2500-ppm Ag sample.

D. Isothermal annealing

For the ≈30-MHz signal, significant annealing of the C_{44}-1 peak occurred during its measurement. The isothermal annealing that occurred at the set point T_A, for each isochronal anneal, was analyzed using Eq. (1). No correction was attempted for the effects of the annealing of the higher-temperature peak upon which this peak rides. These effects might be significant. Here the values $E_M=0.253$ eV and $\nu/N\approx 9.95\times 10^6\ \mathrm{s}^{-1}$ are obtained.

E. Isochronal annealing

The percentages of the C_{44}-1 and C' peaks remaining are plotted against isochronal anneal temperature in Fig. 9. The annealing of the C_{44}-1 peak appears to lag behind that of the C' peak by ≈2.7 K. As in the case of Al-Si, one is again confronted with the question of whether or

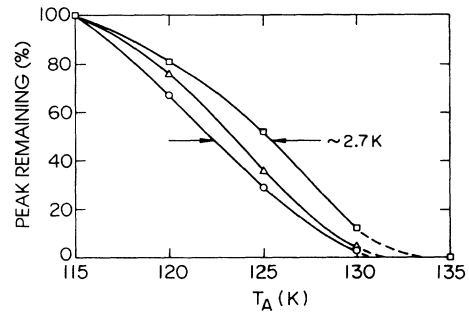

FIG. 9. Al–1280-ppm Ag. Percentage of the initial peak height remaining after successive isochronal anneals at $T=T_A$ for the C' peak (○), C_{44}-1 (□), and that predicted using the first-order parameters $E_M=0.253$ eV and $\nu/N\approx 9.95\times 10^6\ \mathrm{s}^{-1}$ (△).

not both peaks result from the presence of a single defect species. Both the bad thermal connection alluded to earlier and the effects of the peak occurring at a higher temperature than C_{44}-1 might have contributed to this 2.7-K shift. In addition, the sample was irradiated on opposite sides during the C' and C_{44} runs. Since the penetration depth of 2.5-MeV electrons in aluminum is approximately 4 mm and the sample dimension parallel to the beam was approximately 1 cm, the concentration gradient within the sample may have led to the observed shift. The isothermal annealing results were used to calculate the expected isochronal curve. This is also plotted in Fig. 9.

VI. Al–2500-ppm Ag

A. Composition

This sample was analyzed by Coors/Spectro-Chemical Laboratory and determined to have a Ag concentration of 2501±250 ppm.

B. C' mode

Velocity measurements were made at 30.4 MHz following irradiation to 4.0 ppm FP. As expected, a dispersion was detected centered at $T_P=22.8$ K. The size of this dispersion was nearly a factor of 9 smaller than that expected on the basis of what was detected in the Al–1280-ppm Ag. In fact, as will be seen below, the C_{44} peaks were also reduced by a similar factor.

C. C_{44} mode

For the C_{44} mode the sample was irradiated with a dose corresponding to 3.6 ppm FP. Attenuation measurements were made at 10.17 and 30.8 MHz simultaneously. Following irradiation, the expected peak, C_{44}-1, was detected at $T_P\approx 101.1$ and 111.1 K for 10.17 and 30.8 MHz, respectively. After irradiation, the peak decrement for the 10.17-MHz signal was $\delta=2.39\times 10^{-5}$ (normalized to 1 ppm FP). As in the C' data, this value is smaller (by about a factor of 7) than expected. This peak is shown for the 30.8-MHz data following the irradiation and several successive isothermal anneals in Fig. 10. The values of Q and τ_0 which characterize this peak are consistent with those obtained with the Al–1280-ppm Ag sample. It is rather curious that (in Fig. 10) one sees no evidence of the peak at higher temperatures as was seen in Fig. 8. This might be due to effects of concentration-dependent annealing and the fact that in this case changes are referenced to the decrement present after the 165-K anneal.

In addition, the small peak near 20 K that was mentioned above was detected. The decrement of this peak, which will be referred to as C_{44}-3, was $\approx 1.7\times 10^{-6}$ (normalized to 1 ppm FP). This value is nearly a factor of 4 smaller than that expected on the basis of the Al–1280-ppm Ag data. This peak had not changed in height following a 165-K anneal, but was annihilated in stage III.

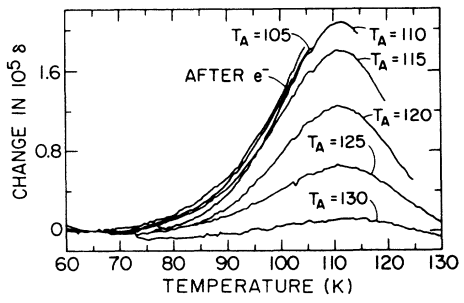

FIG. 10. Al–2500-ppm Ag, 30.8-MHz, C_{44}-1 peak following irradiation and after successive isochronal anneals. The peak is relative to the log decrement present after a 165-K anneal.

D. Isochronal annealing

The annealing of both the C' and C_{44}-1 peaks shifted down in temperature by 2.25 K with the increase in solute concentration (1280→2500 ppm). Again, however, the annealing of the C_{44}-1 peak lagged behind that of the C' by a few degrees kelvin. The 2.5-K shift with concentration is in agreement with that calculated if one uses the first-order parameters determined for Al–1280-ppm Ag and corrects for the change in concentration as suggested earlier in the discussion of Al–36-ppm Si.

VII. SUMMARY OF RESULTS

A. Peak structure

The various e^--irradiation-induced attenuation peaks detected in Al-Si and Al-Ag are represented by bars in Fig. 11. Each bar is located on the temperature scale where one would expect the corresponding peak to occur

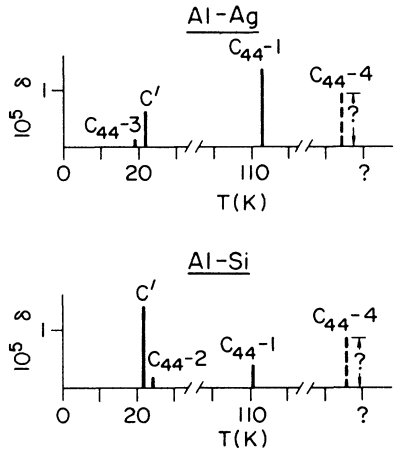

FIG. 11. Representation of the peak structure detected in Al-Si and Al-Ag. Each bar represents a peak at that temperature (for $f=30$ MHz). The length of each bar corresponds to the relative height of each peak. The labels given to each bar serve to indicate the peak mode and to distinguish it from the other peaks. The data in both Al-Si and Al-Ag pointed toward the existence of the C_{44}-4 peak, but its relative height and precise location were not determined.

for a measurement frequency of 30 MHz. In the C' mode only one peak was detected in each sample, and it is labeled accordingly. In the C_{44} mode several peaks were detected in each sample, and they are each given a number. The height of each bar corresponds to the height of the peak it represents following a 1-ppm FP e^- dose. The ultrasonic data in both Al-Si and Al-Ag pointed toward the existence of a peak labeled C_{44}-4, but its relative height and precise location were not determined, as indicated in the figure.

The peak structure of Al-Si is similar to that of Al-Ag in several ways. In both samples, a single C' peak is detected near 20 K, a C_{44} peak (C_{44}-1) is detected near 110 K, and both the C' and C_{44}-1 peaks appear to be due to the presence of a single defect species which exhibits stage-II annealing. In addition, in both samples, the C_{44}-1 peak appears to be riding on the tail of a higher temperature peak, C_{44}-4, which annealed away before it was surmounted. There are also several differences between the peak structures of the two alloys. In Al-Si, the C' peak is significantly larger than C_{44}-1, whereas, the opposite is true for Al-Ag. In Al-Si, one or more small C_{44} peaks, labeled C_{44}-2, are detected near 20 K which appear to anneal in conjunction with the C' peak and C_{44}-1. Conversely, in Al-Ag, a small C_{44} peak, labeled C_{44}-3, is also detected near 20 K. This peak, however, remains until stage III.

B. Activation energy and τ_0

For both alloy systems, the C' and C_{44}-1 peaks were studied in detail. These peaks were well characterized by the equations of Debye assuming an Arrhenius relaxation time with the following parameters:

Sample	Peak	Q (eV)	τ_0 (10^{-13} s)
Al-Si	C_{44}-1	0.112±0.003	0.55±0.08
	C'	0.020±0.001	0.92±0.02
Al-Ag	C_{44}-1	0.105±0.002	1.05±0.33
	C'	0.020±0.002	0.90±0.02

C. Migration energy and prefactor

The annealing of the defect responsible for the C' peak, C_{44}-1, and possibly C_{44}-2 was determined to obey first-order kinetics with the following parameters:

Sample	E_M (eV)	v/N (10^7 s^{-1})
Al–673-ppm Si	0.234	0.599±0.12
Al–1280-ppm Ag	0.253	≈0.995

The term v is a product of an attack frequency v_0 and an entropy factor.[19] The computer-simulation work of Dederichs *et al.*[20] included a calculation of the local frequency spectrum of ⟨100⟩ self-interstitial dumbbells. This spectrum includes several low-frequency resonances, the lowest of which has a resonant frequency $\omega_R \approx (\frac{1}{10})\omega_{max}$. One might then estimate $k\Theta_D/10 \approx h\nu_0$, where k is Boltzmann's constant, $\Theta_D \approx 400$ is the Debye

temperature for Al, and h is Planck's constant, so that $v_0 \approx 10^{12}$. The concentration dependence of the annealing suggests that the number of equivalent jumps to a sink, N, be set equal to the inverse of the solute concentration ($\approx 10^3$), so that $v_0/N \approx 10^9$. There remains a discrepancy of 2 orders of magnitude. It might be that the entropy factor could lead to agreement between this estimate and the results reported above.

D. Diaelastic effect

For Al–673-ppm Si, the diaelastic effect, which annealed in conjunction with the C_{44}-1 and the C' peaks, was measured. The magnitude of the relative elastic constant change per unit concentration of defects, γ, due to this effects was

$$\alpha_{44} = \frac{\partial \ln C_{44}}{\partial \gamma} \approx -35, \quad \alpha' = \frac{\partial \ln C'}{\partial \gamma} \approx -13 \ .$$

Here one might note that these values are similar to the values $\alpha_{44} = -27$ and $\alpha' = -16$ reported by Robrock and Schilling[21] for ⟨100⟩ self-interstitial dumbbells in pure aluminum.

VIII. COMPARISON WITH PREVIOUS WORK

A. Resistivity results

Early measurements of resistivity changes with annealing after irradiation did not yield a characteristic pattern for stage-II recovery. Following neutron irradiation at 78 K a single recovery substage was detected near 125 K for both Al–1000-ppm Ag and Al–1000-ppm Si by Ceresara *et al.*[22] On the other hand, Garr and Sosin[23] found no distinct recovery substages in 1-MeV e^--irradiated Al–1000-ppm Ag, which could be associated with the addition of the solute. A small recovery substage near 125 K was attributed to the presence of residual impurities.

More recently, a clearer spectrum has been established for electron irradiation with measurements by Dworschak *et al.*[24] and by Maury *et al.*[25] Dworschak *et al.* detected two stage-II substages in Al–50-ppm Ag after 3-MeV electron irradiation at 54 K. The first occurs near 130 K, and a smaller and narrower one occurs near 160 K. Maury *et al.*, using 1.6- and 0.8-MeV e^- irradiation on Al–15-ppm Ag, Al–59-ppm Ag, and Al–135-ppm Ag, find similar results, except they find evidence that the larger annealing stage at lower temperature may be composed of two substages (II_A and II_B) located near 122 and 132 K for 135 ppm Ag. All of these substages move to lower temperatures with increasing Ag content. In addition, the size of the substages decreased with increasing Ag content, increasing e^- energy, and decreasing irradiation temperature.

In ultrasonic measurements, the C' peak, C_{44}-1 (Fig. 9), and possibly also the minor peak C_{44}-2, anneal away near 125 K for 1280 ppm. This annealing occurs at lower temperatures for higher concentrations. By extrapolating either the resistivity data of Maury *et al.* to higher concentrations or the present ultrasonic data to lower concentrations, it appears that the ultrasonic recovery stage corresponds to stage II_B of the resistivity recovery, although the ultrasonic recovery temperature range is somewhat wider than II_B, and may possibly include II_A.

Maury *et al.* make a quantitative fit of their data to a model for stage-II recovery in terms of the relative populations of various defects (vacancies, trapped single interstitials, trapped di-interstitials, etc.), capture radii, and resistivity assignments for the various defects. As a result, they conclude that trapped di-interstitials recover in stage II around 130 K for Al-Ag and that mixed interstitials are stable up to at least 180 K. This conclusion is in contrast and contradiction to the conclusion and interpretation in the present paper, according to which mixed interstitials anneal in stage II near 130 K (128 K for 1280 ppm and 125 K for 2500 ppm). We therefore summarize the evidence for this viewpoint following a brief review of results obtained from other measurements.

B. EXAFS

The extended x-ray-absorption fine-structure spectroscopy (EXAFS) technique was applied by Weber and Peisl[26] to Al–400-ppm Ag, following e^- irradiation near 85 K. Two defect structures were detected. The first was present following irradiation, was reduced following a 120-K anneal and was gone following a 165-K anneal. The radial distance between the Ag atom and closest Al atom comprising this structure is given as 2.34 Å. The annealing behavior of this defect structure is consistent with that of the defect species responsible for the C', C_{44}-1, and C_{44}-2 peaks. The fact that only one defect structure was detected that exhibited this annealing behavior supports the view that these peaks are the result of the presence of a single defect species. The second defect structure detected appeared to grow in following the 165-K anneal, but disappeared after a 185-K anneal. The behavior of this defect structure is consistent with that responsible for the peak labeled C_{44}-4.

C. Channeling measurements

Al-Ag alloys, of various dilute Ag concentrations, have been studied using the channeling technique.[27–31] In these studies, Ag atoms are reported to trap interstitials forming ⟨100⟩ mixed dumbbells which anneal during stage III. This annealing behavior is consistent with that of the C_{44}-3 peak. A ⟨100⟩ mixed dumbbell, however, having tetragonal symmetry, would not give rise to a peak in the C_{44} mode.

D. Internal friction measurements

Internal friction measurements performed on polycrystalline Al–700-ppm Ag and Al–900-ppm Si by Takamura and Kobiyama[4] confirm the existence and behavior of the C' and C_{44}-1 peaks of Fig. 11. In Al-Ag, using a 1519-Hz signal, two peaks, which annealed together, near 125 K, were detected at 11.3 and 58 K, respectively. These peaks grow in during stage II_E. In addition, a peak, which was annihilated following a 103-K anneal, was detected at 66 K. Takamura and Kobiyama identify

this 66-K peak as corresponding to C_{44}-1; however, the annealing behavior exhibited by this 66-K peak is inconsistent with that of C_{44}-1. In addition, using the values of τ_0 and Q obtained for the C_{44}-1 peak in Al-Ag, one would expect C_{44}-1 to occur at 58.4 K for a 1519-Hz signal. Consequently, one would identify the 58-K peak detected by Takamura and Kobiyama as corresponding to C_{44}-1. The parameters obtained for the C' peak in Al-Ag indicate that it should occur near 11 K for a 1519-Hz signal in agreement with the internal friction results. In Al-Si, using a 741-Hz signal, two peaks which annealed together were detected at 12.8 and ≈ 57 K. These temperatures correspond to those expected for the C' and C_{44}-1 peaks, respectively, on the basis of the parameters obtained in this study. In addition to the peaks corresponding to the C' and C_{44}-1 peaks in Al-Ag and Al-Si, several small peaks (including the 66-K peak mentioned above) appear in the internal friction data for both alloys. It may be that the annealing behavior of one of these peaks is consistent with that of C_{44}-4.

IX. DISCUSSION

Evidence that the 130-K annealing in Al-Ag corresponds to mixed interstitials and not to trapped di-interstitials as concluded by Maury *et al.*, comes from the following. Firstly, the EXAFS determination of Weber and Peisl[26] of 2.34 Å as the radial distance between the Ag atom and the nearest Al atom is consistent with a mixed interstitial, and not with a trapped interstitial structure, for which one would expect a distance close to $a/\sqrt{2}=2.86$ Å.

Secondly, the internal friction measurements of Takamura and Kobiyama[4] show that the defect annealing near 130 K is created during stage I_E, and is not directly produced by the irradiation.

Thirdly, the diaelastic effects found here are very large and anneal in the same stage-II temperature range where the relaxation peaks disappear. This can be understood if it is supposed that this annealing corresponds to mixed dumbbells migrating to impurities. In such a process there could be a relatively small resistivity change and large diaelastic change if the resistivity of a mixed dumbbell plus an isolated silver atom differs little from the resistivity of an Al-Ag-Ag complex. On the other hand, if only 10–20% of the defects (trapped di-interstitials) anneal while the majority (90–80%) of defects (mixed dumbbells) do not, then the trapped di-interstitials would have to have a diaelastic polarizability of 10–5 times larger than the values obtained, which are already somewhat larger than is found for self-interstitials. This seems extremely unlikely.

Fourthly, there is no independent evidence for a sizable fraction of Frenkel-pair clusters for 3-MeV e^- irradiation. Ehrhart and Schilling[32] found evidence for an average interstitial cluster size of two at the end of stage I in pure Al, but found no evidence for clusters created by the radiation at lower temperatures.

The conclusions reached by Maury *et al.*, while based on a quantitative fit to a damage production model for the resistivity changes, are nonetheless model dependent. Alternative models which also explain the concentration, energy, irradiation temperature, and dose dependence can be devised which at least qualitatively describe the data. For example, it might be supposed that for high-impurity concentrations those interstitials which could otherwise lead to correlated recovery (stage I_D) might become trapped as mixed dumbbells in the strain field of a vacancy which prevents their annealing and rotation. Then the fraction of mixed dumbbells which are isolated and able to rotate (giving rise to anelastic relaxation peaks) and migrate in stage II will be reduced with increasing impurity concentration, decreasing e^- energy, and decreasing irradiation temperatures.

For the reasons given above we proceed under the assumption that the relaxation peaks and diaelastic effects observed arise from a mixed dumbbell and examine next the limitations on the possible form of such a dumbbell provided by the observed polarization dependence of the effects.

A. Selection rules

The selection rules governing the anelastic response of point defects in cubic crystals are summarized in Table I. The first column lists the defect symmetry which is determined by the group of elements common to both the defect when isolated from the crystal and the site in the perfect lattice occupied by the defect. The total number, n_t, of stress-distinguishable defect orientations for each defect symmetry is given in the second column. Nowick[33] describes a scheme whereby each of the n_t orientations is labeled $1 \rightarrow n_t$. In this same reference, the relaxation times τ, for each of the (C_{44} and C') stress-active modes is expressed in terms of the rate of reorientation, ν_{1J}, between the distinguishable defect orientation labeled 1 and each of the others, labeled J ($J=2 \rightarrow n_t$). These relaxation times are listed in the third and fourth columns of Table I, where an entry of "none" indicates that a relaxation in that mode is ruled out on the basis of symmetry.

B. Tetragonal complexes

Table I indicates that evidence for the presence of a tetragonal defect species in e^--irradiated Al-Si and Al-Si would consist of a C' peak with no counterpart in the C_{44} mode. A C' peak was detected in both alloys; however, the C_{44}-1 and C_{44}-2 peaks annealed together with this peak.

C. Trigonal complexes

If a trigonal complex was present, one might expect to detect a C_{44} peak with no counterpart in the C' mode. A peak consistent with this expectation was detected in Al-Ag and labeled C_{44}-3. The calculations of Dederichs *et al.*[20] indicated that for undersized impurities such a complex would be strongly bound. The C_{44}-3 peak remained undiminished until stage III, but Ag is slightly oversized in the Al lattice.[34] Si, on the other hand, is nearly 16% undersized in the aluminum lattice and no

TABLE I. Selection rules for anelasticity in cubic crystals.

Defect symmetry	n_t	C_{44}	C'
cubic	1	none	none
tetragonal	3	none	$\tau^{-1}=3\nu_{12}$
trigonal	4	$\tau^{-1}=4\nu_{12}$	none
⟨100⟩ orthorhombic	6	none	$\tau^{-1}(1)$, $\tau^{-1}(2)$
⟨110⟩ orthorhombic	6	$\tau^{-1}=2\nu_{12}+4\nu_{13}$	$\tau^{-1}=6\nu_{13}$
⟨100⟩ monoclinic	12	$\tau^{-1}(3)$	$\tau^{-1}(4)$, $\tau^{-1}(5)$
⟨110⟩ monoclinic	12	$\tau^{-1}(6)$, $\tau^{-1}(7)$	$\tau^{-1}(8)$
triclinic	24	$\tau^{-1}(9-11)$	$\tau^{-1}{}_{12}$, $\tau^{-1}{}_{13}$

$$\tau^{-1}(1,2)=(\nu_{12}+3\nu_{13}+\nu_{14}+\nu_{16})\pm(1/\sqrt{2})[(\nu_{12}-\nu_{14})^2+(\nu_{14}-\nu_{16})^2+(\nu_{12}-\nu_{16})^2]^{1/2}$$
$$\tau^{-1}(3-5)=\text{values not given}$$
$$\tau^{-1}(6,7)=[\nu_{17}+3\nu_{12}+5\nu_{13}+\tfrac{3}{2}(\nu_{15}+\nu_{16})]\pm\{[\nu_{12}-\nu_{13}-\nu_{17}+\tfrac{1}{2}(\nu_{15}+\nu_{16})]^2+2(\nu_{15}-\nu_{16})^2\}^{1/2}$$
$$\tau^{-1}(8)=6\nu_{13}+3\nu_{15}+3\nu_{16}$$
$$\tau^{-1}(9-13)=\text{values not given}$$

such peak was detected. In addition, one cannot conclude that the defect symmetry of the complex responsible for the C_{44}-3 peak is trigonal, as there may have been other peaks associated with this defect, which were outside the range of detection in this study. One can, however, exclude defect complexes which display tetragonal or ⟨100⟩ orthorhombic symmetry.

D. Orthorhombic complexes

It is often supposed that an oversized impurity would trap an interstitial forming a ⟨110⟩ orthorhombic symmetry complex.[20] If a ⟨110⟩ orthorhombic defect species was present in the sample, one might expect to detect one C' peak and one C_{44} peak. The relaxation times associated with these peaks (Table I), however, are such that one would expect to see either both peaks at about the same temperature or low-temperature C_{44} peak and a high-temperature C' peak. Therefore, a defect of this symmetry cannot account for the observation of the C' and C_{44}-1 peaks. For a ⟨100⟩ orthorhombic complex one might observe two C_{44} peaks with no counterpart in the C' mode. This symmetry is, therefore, inconsistent with the observation of the C' peak.

E. Monoclinic complexes

If a defect species with ⟨100⟩ monoclinic symmetry was present, one might expect to see two C' peaks and one C_{44} peak. One might attribute the C' and C_{44}-1 peaks to such a complex and assume the other C' peak was not detected. The computer work of Dederichs *et al.* revealed the possibility of two metastable complexes of ⟨100⟩ monoclinic symmetry (C_{1h}). The weak binding of these complexes would be consistent with stage-II annealing. The calculation, however, indicated that such complexes would only be formed for undersized impurities, whereas Ag is oversized.

The fact that the peak(s) labeled C_{44}-2 appeared to anneal in conjunction with both the C' and C_{44}-1 peaks suggests strongly that the defect complex exhibits ⟨110⟩ monoclinic symmetry. Table I indicates that such a complex would be characterized by three relaxation times. Consideration of the case, where ν_{15} dominates the other rates, yields

$$\tau^{-1}(C')\approx 3\nu_{15}+(6\nu_{13}+3\nu_{16}) , \quad (2)$$

$$\tau^{-1}(C_{44})_1\approx 3\nu_{15}+\tfrac{1}{3}(10\nu_{12}+14\nu_{13}+2\nu_{17}+\nu_{16}) , \quad (3)$$

$$\tau^{-1}(C_{44})_2\approx \tfrac{4}{3}(2\nu_{12}+4\nu_{13}+\nu_{17}+2\nu_{16}) . \quad (4)$$

On the basis of these relaxation times, one would expect a low-temperature peak in both the C' and C_{44}, peaks occurring at slightly different temperatures (with $\tau^{-1}\approx 3\nu_{15}$), and a higher-temperature C_{44} peak. The relations in Table I used to generate Eqs. (2)–(4) are symmetric in ν_{15} and ν_{16}, so that a similer result is obtained if one assumes ν_{16} to be the dominant rate.

F. Proposed model

In addition to having proper symmetry, a suitable model would have to contain a provision for the change in the $(C')/(C_{44}\text{-}1)$ peak height ratio with solute (Ag→Si) and the fact that the C_{44}-2 peak was not detected in Al-Ag. A 24-state, ⟨110⟩ monoclinic, mixed-dumbbell model which meets these requirements has already been introduced.[34] One might expect a mixed-dumbbell complex to have a diaelastic polarizability of similar anisotropy and magnitude as that of a self-interstitial dumbbell as was observed (Sec. VII). Three possible cages for this defect, consisting of jump processes labeled *A*, *B*, and *C* are discussed. At temperatures where all three jump processes would occur readily, the dumbbell could be expected to exchange self-interstitial atoms, resulting in long-range migration of the solute as was suggested by the observed solute concentration-dependent annealing. In light of the above discussion, one can identify *A* jumps with ν_{15}, *B* jumps with ν_{12}, and *C* jumps with ν_{16}. In addition, this model can be easily adjusted to accommodate the 2.34-Å radial distance parameter determined by EXAFS alluded to earlier.

X. CONCLUSION

Electron irradiation of dilute alloys of Al-Si and Al-Ag gives rise to a similar ultrasonic attenuation peak spectrum in both alloys. The data presented here are consistent with much of what has been reported by other workers.[4,22–31] In addition, new information in the form of activation energies, jump rates, migration energies, possible annealing mechanisms, diaelastic effects, and polarization dependence are reported. The basic characteristics of these peaks are summarized in Sec. VII. The peaks labeled C', C_{44}-1, and C_{44}-2 (Fig. 11) appear to anneal in unison suggesting that they arise from the presence of a single defect structure. A ⟨110⟩ monoclinic mixed-dumbbell defect complex has been proposed that can account for the major characteristics of these peaks.

ACKNOWLEDGMENTS

This work was supported by the U.S. Department of Energy, Division of Materials Sciences, Contract No. DE-AC02-76ER091198. One of the authors (A.V.G.) thanks the Los Alamos National Laboratory, where he received support from the Bernd T. Matthias Visiting Scholar Program while this manuscript was being completed.

*Current address: The Aerospace Corporation M2/250, P.O. Box 92957, Los Angeles, CA 90009.
†Permanent address.

[1]A. V. Granato, J. Holder, K. L. Hultman, D. L. Johnson, G. G. Setser, P. Wallace, and H. Wong, in *Point Defects and Defect Interactions in Metals,* edited by J. Takamura *et al.* (University of Tokyo Press, Tokyo, 1982), p. 360.
[2]K. L. Hultman, J. Holder, and A. V. Granato, J. Phys. (Paris) Colloq. C5-753 (1981).
[3]E. C. Johnson and A. V. Granato, J. Phys. (Paris) Colloq. C10-63 (1985).
[4]S. Takamura and M. Kobiyama, Radiat. Eff. **91**, 21 (1985).
[5]A. S. Nowick and B. S. Berry, *Anelastic Relaxation in Crystalline Solids* (Academic, New York, 1972).
[6]T. Ochs, J. Sci. Instrum. (J. Phys. E) **1**, 1122 (1968).
[7]W. L. Johnson, Ph.D. thesis, University of Illinois, 1987.
[8]E. C. Johnson, Rev. Sci. Instrum. **58**, 2295 (1987).
[9]E. C. Johnson, Rev. Sci. Instrum. **59**, 188 (1988).
[10]D. L. Johnson, Ph.D. thesis, University of Illinois, 1978.
[11]W. Schilling, J. Nucl. Mater. **69&70**, 465 (1978).
[12]K. L. Hultman, Ph.D. thesis, University of Illinois, 1979.
[13]A. V. Granato and T. G. Nilan, Phys. Rev. **137**, A1250 (1965).
[14]E. C. Johnson, Ph.D. thesis, University of Illinois, 1987.
[15]E. C. Johnson and A. V. Granato, in *Phonon Scattering in Condensed Matter V,* edited by A. C. Anderson and J. P. Wolfe (Springer-Verlag, Berlin, 1986), p. 100.
[16]F. R. Fickett, Cryogenics **11**, 349 (1971).
[17]A. B. Pippard, Rep. Prog. Phys. **23**, 176 (1960).
[18]P. W. Wallace, Ph.D. thesis, University of Illinois, 1983.
[19]G. H. Vineyard, J. Phys. Chem. Solids **3**, 121 (1957).
[20]P. H. Dederichs, C. Lehmann, H. R. Schober, A. Scholz, and R. Zeller, J. Nucl. Mater. **69&70**, 176 (1978).
[21]K.-H. Robrock and W. Schilling, J. Phys. F **6**, 303 (1976).
[22]S. Ceresara, T. Federighi, and F. Pieragostini, Phys. Lett. **6**, 152 (1963).
[23]K. R. Garr and A. Sosin, Phys. Rev. **162**, 669 (1967).
[24]F. Dworschak, Th. Monsau, and H. Wollenberger, J. Phys. F **6**, 2207 (1976).
[25]F. Maury, A. Lucasson, P. Lucasson and C. Dimitrov, J. Phys. F **18**, 657 (1988).
[26]W. Weber and H. Peisl, in *Point Defects and Defect Interactions in Metals,* Ref. 1, p. 368.
[27]M. L. Swanson and F. Maury, Can. J. Phys. **53**, 1117 (1975).
[28]M. L. Swanson and L. M. Howe, in *Point Defects and Defect Interactions in Metals,* Ref. 1, p. 364.
[29]L. M. Howe and M. L. Swanson, in *Point Defects and Defect Interactions in Metals,* Ref. 1, p. 53.
[30]N. Matsunami, M. L. Swanson, and L. M. Howe, Can. J. Phys. **56**, 1057 (1978).
[31]M. L. Swanson, L. M. Howe, and A. F. Quenneville, J. Phys. F **6**, 1629 (1976).
[32]P. Ehrhart and W. Schilling, Phys. Rev. B **8**, 2604 (1973).
[33]A. S. Nowick, Adv. Phys. **16**, 1 (1967).
[34]H. W. King, J. Mater. Sci. **1**, 79 (1966).
[35]E. C. Johnson and A. V. Granato, J. Mater. Sci. Forum **15-18**, 581 (1987).